Proceedings of the ASME 2024
51st Annual Review of Progress in
Quantitative Nondestructive Evaluation
QNDE2024
July 22-24, 2024, Denver, Colorado

QNDE2024-135272

DETERMINATION OF STRUT QUALITY FACTORS IN ADDITIVELY MANUFACTURED LATTICES USING IN-SITU COMPRESSION TESTING µ-CT

Vincent DiNova[1], H.B. Flynn[1], Paul Korinko[1], David Immel[1]

[1]Savannah River National Laboratory, Aiken, SC

ABSTRACT

In response to the need for an automated, commercial method to qualify additively manufactured (AM) lattice components, an experiment was conducted to evaluate the effects of defective lattice struts on the structural compression strength. Lattice samples with known defective or missing struts were compressed using a Deben CT5000RT and imaged using x-ray µ-CT. The compressive force and x-ray computed tomography results were compared to defect free standards to evaluate the impact of each defect type on the overall structure's compressive strength. This analysis will allow for simplifications to Finite Element Analysis (FEA) on AM parts without sacrificing model fidelity. Understanding the contribution of each defect type and severity will also better inform non-destructive evaluation (NDE) personnel of the inspection parameters necessary to detect the smallest feature of importance.

Keywords: Additive Manufacturing; X-Ray Computed Tomography; Lattice; Defect; Compression Testing

1. INTRODUCTION

Additive Manufacturing (AM) technology has matured over the last decade, making it possible to design and manufacture components that are not possible by traditional methods [1]. One promising application utilizes 3D lattice structures, which offer a reduction in weight and material without sacrificing structural integrity [2-3]. In the automotive and aerospace industries, reducing weight and material expenses are driving factors to the innovation of AM lattice technologies.

One major hurdle to mainstream adaptation is the variability of AM printing. AM lattice structures commonly have issues with porosity [5-6], surface roughness [7-8], strut waviness and variability [9-10]. Characteristics inherent to the AM printing process can also lead to lack of fusion and un-sintered powder that does not contribute to the structural integrity of the parts.

This variability in AM parts will likely require unique inspection techniques before certifying a part is acceptable to be used. AM lattice structures present an additional challenge since any local defect can add stresses that propagate globally. To inspect internal defects of an AM part, x-ray Computed Tomography (CT) is often used [4]. X-ray CT is a nondestructive examination technique that acquires images from multiple angles to reconstruct a representation of the inspected part.

X-ray CT scan data is fed into reconstruction algorithms to produce a digital 3D rendering of the object. A common commercial reconstruction software used is Volume Graphics. Along with the reconstruction software, Volume Graphics offers add-ons to quantify porosity and grain structures, make comparisons between as-designed and as-built components, mesh generation, and finite element analysis (FEA). Due to the complex surface features created by AM, generating a mesh to capture the geometry of AM parts is computationally difficult, leading to prohibitive run times. These long run times will make qualification of as-built parts difficult by using these commercial tools.

Improvements to lattice designs and printing techniques have been explored for decades [11-12]. Commonly, FEA is deployed to compare with mechanical testing to model the response. As additive manufacturing improves, it is vital that inspection methods are developed to overcome the challenges of evaluating parts with such inherently high variability.

In this article, metal Ti-6Al-4V lattices were designed and built with the inclusion of geometric defects of a wide variety to help

establish a qualification process for AM lattices. Each lattice was prepared on a single build plate to limit process variability. Compression testing and μ-CT scans were taken to capture the accurate geometry of the as-built components and to determine the load required to fracture the defective strut. Beam elements of comparable strength can be substituted in the as-designed component to perform a more reasonable FEA analysis without overburdening computational resources.

2. MATERIALS AND METHODS

2.1 Lattice Defect Design

To test the mechanical response of individual defects, single unit cell lattices were designed to include commonly observed lattice defects of varying sizes and magnitude of 25%, 50%, and 75%: slant, extra, wave, thin (rapid, medium, and long lengths), and kinked (centered, shifted, and centered with a diameter change). This design process was done using COMSOL ver. 5.0. Each defect was printed eight times in separate lattices for repeatability of testing. Additionally, a set of eight standard lattices with no defects and eight lattices with a missing strut were printed. Figure 1 illustrates the size and type of defects generated.

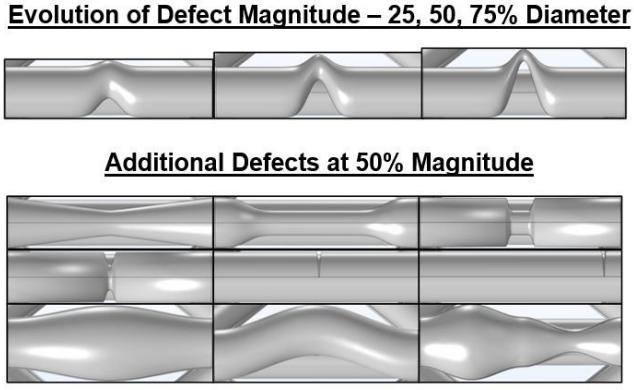

Figure 1: (top) Image displaying kink + diameter change of defect magnitude 25% - 75%. (bottom) Image displaying different types of defects at a magnitude of 50%. Each defect in order from left to right: Thin, Long Thin, Rapid Thin, Sharp, Crack, Shifted Crack, Extra, Wave, and Thick to Thin.

The lattices were each designed to be 2.5mm tall, with a strut length of 3.73mm, and a strut diameter of 50mm. To ensure uniform compression, a top and base plate of 0.75mm thickness was added. Compression testing in the Deben CT5000RT requires samples to be between 5mm and 15mm, so all dimensions were scaled 3x to meet the system stroke length.

2.2 Sample Generation

256 total lattices were printed using Ti-6Al-4V on a single build plate on a GE ARCAM A2X. The samples were spaced such that no residuals from adjacent lattices will affect the surrounding lattices.

The first task was to preheat the bed to 730 °C with a beam speed of 13000 mm/s and a current of 38 mA. The hatch spacing was set for a depth of 0.09 mm and a line offset of 1.2 mm.

For the melt phase, the beam speed and current were lowered to 4530 mm/s and 20 mA to achieve a surface temperature of 650 °C. The hatch spacing was lowered to a depth of 0.05 mm with an offset of 0.2 mm.

For the lattice samples, the beam speed was lowered to 1500 mm/s with a current of 3 mA to achieve a surface temperature of 750 °C with a depth of 0.07 mm and line offset of 0.2 mm. To build the support structure, the beam speed was set to 1600 mm/s at a current of 5.5 mA.

After the samples were printed and cooled, they were cut from the build plate, and the bases of the samples were filed down to remove residual uneven surfaces for compression testing, Figure 2.

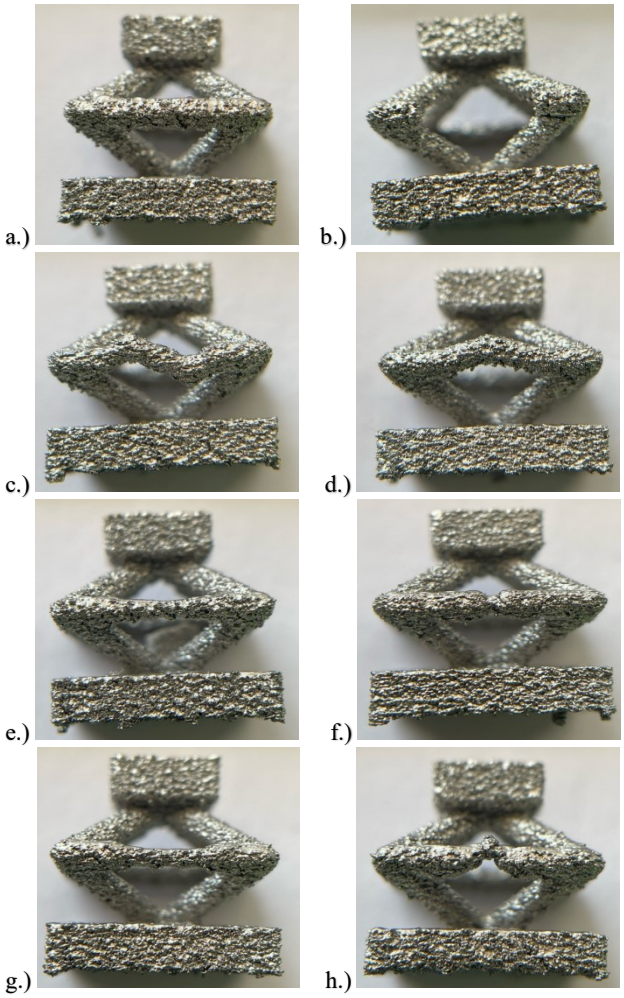

i.) 

Figure 2: As built defect lattices for conditions: a) Standard b) Missing Strut, c) Slant 50%, d) Wave 50%, e) Thin 25%, f) Rapid Thin 50%, g) Long Thin 25%, h) Kink+Diameter 50%, i) Shifted Kink 75%

2.3 X-ray Scanning and Compression Testing

Each lattice was CT scanned prior to undergoing compression testing. CT scans were performed using an X-Ray Worx XWT-225-TCNF with a source-to-object distance of 112.33 mm and a source-to-detector distance of 561.66, resulting in a magnification of 5x. The flat panel used was a Varex XRD 1611 AP3 with a 100-micron pixel pitch, resulting in a nominal pixel size of 20 µm after magnification.

The scans were performed with eight samples mounted on a single holder, with two layers of four lattices, separated by low density foam. 1800 images at 200 keV at 20W were taken for each scan.

A Deben CT5000RT *in-situ* compression stage was mounted to the rotational stage inside the CT booth, Figure 3. The Deben CT5000RT has an x-ray window that allows for x-rays to pass through while compressing. To prevent movement during the scans, a fixed displacement was used in between scans. To accommodate the size of the Deben CT5000RT, the source to object distance was moved to 197.73 mm, resulting in a magnification of 2.84X and a nominal pixel size of 35.2 µm.

Figure 3: Experimental Setup with Deben CT5000RT Mounted in CT Booth

For the first scan of each sample, the compression jaws were opened fully to 15mm, the sample was loaded into the loadcell, and the offset was reset to 0. The goto setting was used to find the initial height by closing the jaws until 5N was registered on the loadcell.

Full CT scans were completed for a standard lattice, missing strut lattice, 50% wave lattice, and a 50% kink with diameter change lattice. After each initial scan, the stage was displaced in 0.25mm increments and scanned again until the sample is fractured.

Compression data was then captured for each additional sample in the Deben CT500RT at a motor speed of 0.50 mm/min and a sample rate of 500ms. The operating mode was set to compression and allowed to run without interruption until the samples began to fracture.

3. RESULTS AND DISCUSSION

3.1 Simulated FEA Results

Displacement simulations were created to form a basis for the experimental design. The effect of each defect was measured as the highest first principal stress in the defective strut with a 1kN, 2kN, and 3 kN load applied to the top platform and compared to a load-free standard. Figure 4 demonstrates the change in displacement and first order stresses for a standard, shifted kink, and missing strut lattice under 0N, 1kN, 2kN, and 3kN fixed load. As expected, larger and more significant defects (mainly thinning, cracks, and kinks) lead to larger localized peak stresses in the lattice structure as the load increases.

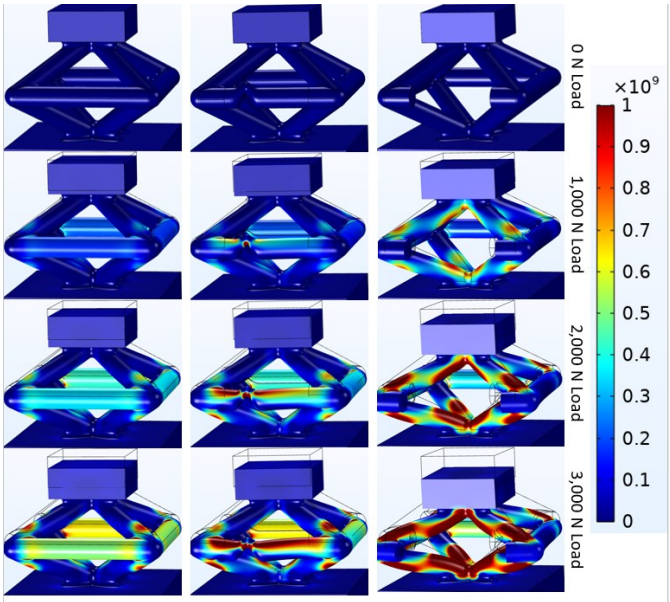

Figure 4: Change in displacement and first order stresses for a standard (top-row), shifted kink (middle-column), and missing (right-column) strut lattice under 0 N, 1 kN, 2 kN, and 3 kN fixed load, respective from top to bottom row.

For the simulations, strut fracture was not accounted for. The defective strut for each defect type was isolated demonstrating that thinning defects and kinks cause the greatest change to relative displacement and relative yield force, as seen in Figure 5. The gray dashed and dotted lines, kinked with a thinner diameter and shifted kink with a thinner diameter, demonstrate the highest change. Cracks, which are essentially a rapid loss of material, demonstrated an identical low relative yield force to the kinked with a thinner diameter defect. It was also observed that extra material lattices result in a lower relative displacement than the standard lattice. This is consistent with expectations. As material is removed, the lattice is expected to perform worse than if material was increased.

a)

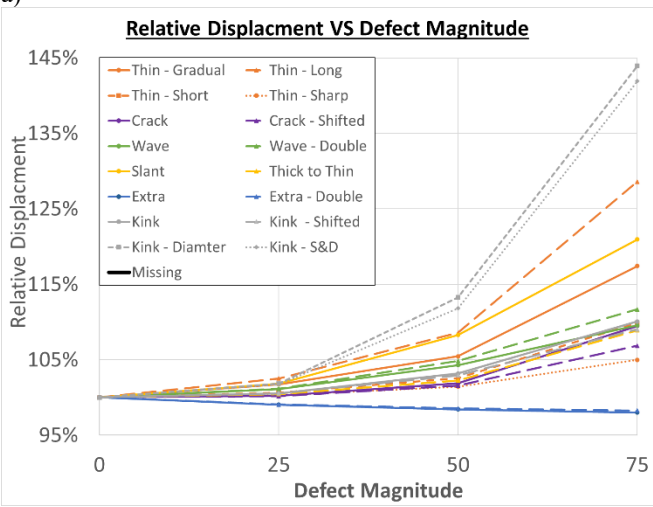

b)

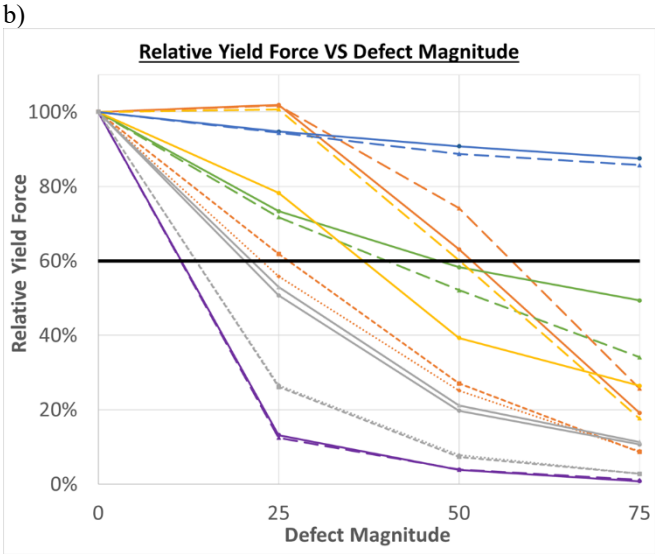

Figure 5: Comparison of lattice defects on resulting: a) displacement and b) relative yield force, compared to standard lattice design

3.2 X-ray CT Results

The CT scans were used to show the progression of fracture and subsequent deformation of the samples. A compressive force is placed on each sample, which places each strut under tension. The Deben CT5000RT records the registered force on the loadcell as well as the total displacement during the trial.

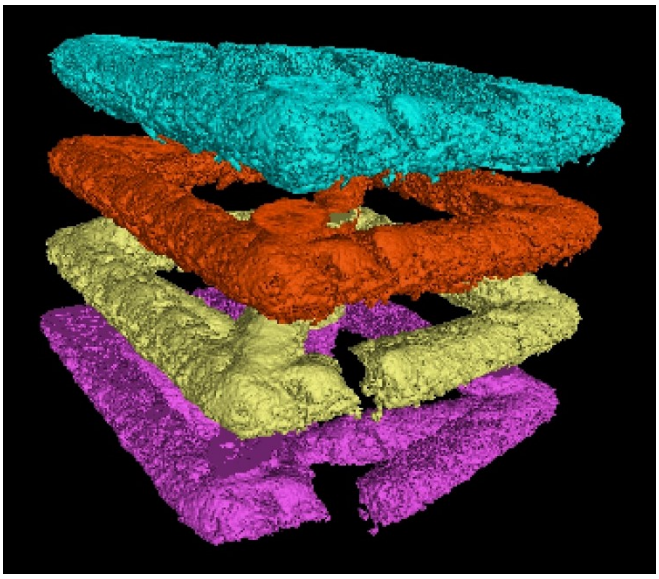

Figure 6: Evolution of fracture in a standard lattice in 0.25 mm increments (top to bottom)

The standard lattice sample, Figure 6, begins fully intact with a surface defect at the fracture location (blue). The compression stage is displaced 0.25 mm (red), which does not cause fracture, but places each strut under tension. After 0.5 mm of displacement (yellow), the location of the surface defect fractures, dispersing the remaining forces throughout the lattice. The balance of forces is now unequal, resulting in deformation away from the fracture location and causing the diagonal struts to bend non-uniformly (purple).

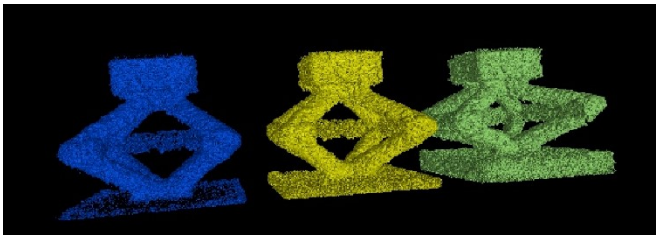

Figure 7: Evolution of deformation in a missing strut lattice in 0.25 mm increments (left to right)

In the missing strut lattice, Figure 7, the sample deforms disproportionally towards the left-hand side. The direction and magnitude of the displaced struts is noticeably similar to the standard sample post-fracture. This result is quantitatively demonstrated in the compression data shown in Section 3.3. The lattices appear to maintain their structure while each strut is

under tension. Once fracture occurs at the weakest point, the lattices deform towards the weakest remaining diagonal strut.

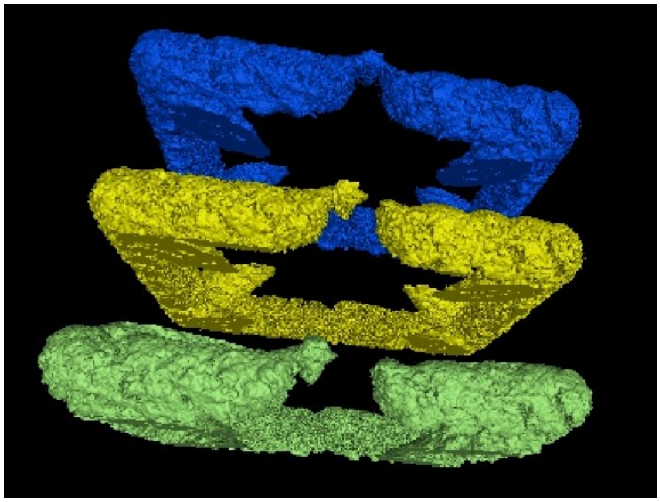

Figure 8: Evolution of fracture in kink+diameter 50% lattice in 0.25 mm increments (top to bottom)

The simulation data showed that the yield point was noticeably lower, in both force and displacement, for the kink with diameter change 50% sample. Figure 8 shows that the test samples followed this simulated response. Here, the strain on the defect causes a fracture in under 0.25 mm. As the compression stage continues, the diagonal struts pull away from the fracture surface, resulting in the weakest remaining strut being shifted downward.

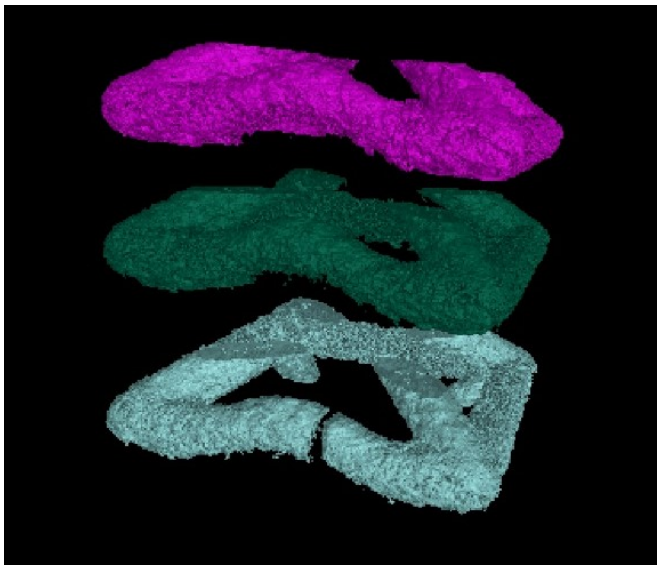

Figure 9: Evolution of fracture in a wave 50% lattice in 0.25 mm increments (top to bottom)

The wave 50% sample, Figure 9, performed in a similar manner to the standard and kink with diameter change 50% samples, even without noticeable surface defects or obvious thin regions. The fracture occurs directly on the wave defect likely due to stress concentrations on the wave surface. The implication for each of these scans is that the fracture occurs in the defect region, meaning these features must be measured during part inspection. It can also be noted that each sample follows the same pattern post-fracture. For AM parts used in repeat operations, incremental scans should be taken to track new breaks in the lattice structure and how the part deforms to compensate for the missing structural load.

3.3 Compression Data

The data output from the Deben CT5000RT is given in force (N) versus displacement (mm). The variability in printing can be observed in the ultimate strength of the samples, Figure 10. Each compression test shows a rise in force until a fracture occurs by brittle failure. Subsequently, the measured force drops, and the lattice begins to plastically deform until the ultimate strength of the samples is reached. The highest registered force in the absence of one strut of the samples was determined to be 1550.9 N with maximum of 1697.2 N, a minimum of 1327.4 N, and a standard deviation of 97.8 N. The large deviation in maximum post-fracture registered force is attributed to the variability in the location and size of cracks and pores seen in the samples.

a)

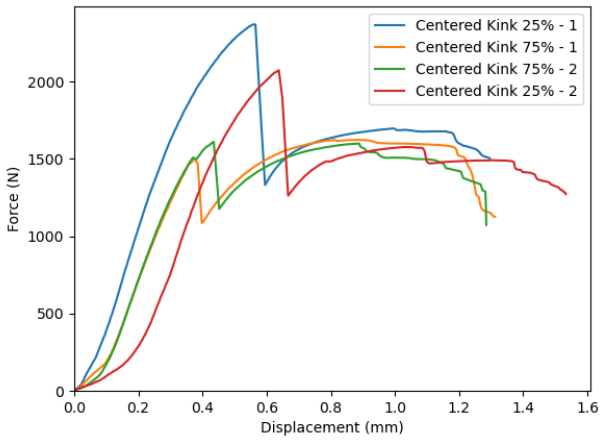

b)

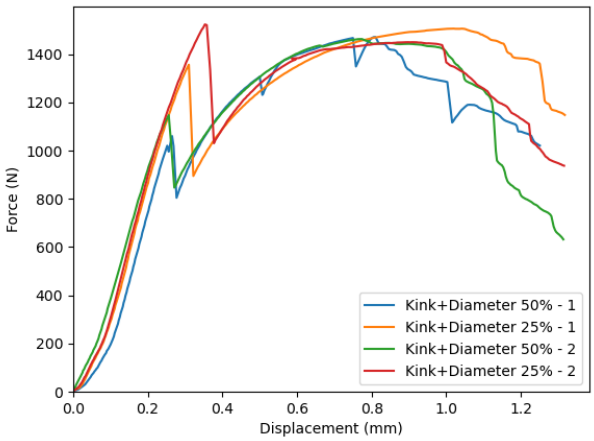
Force (N)
Displacement (mm)
Kink+Diameter 50% - 1
Kink+Diameter 25% - 1
Kink+Diameter 50% - 2
Kink+Diameter 25% - 2

c)

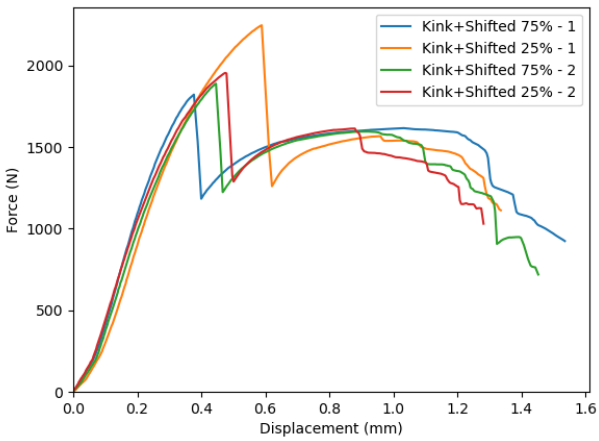
Force (N)
Displacement (mm)
Kink+Shifted 75% - 1
Kink+Shifted 25% - 1
Kink+Shifted 75% - 2
Kink+Shifted 25% - 2

d)

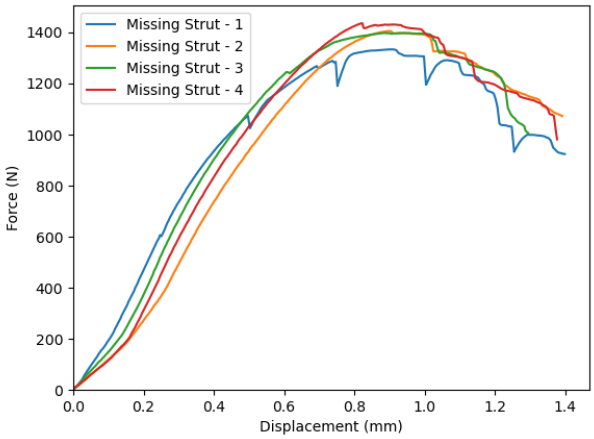
Force (N)
Displacement (mm)
Missing Strut - 1
Missing Strut - 2
Missing Strut - 3
Missing Strut - 4

e)

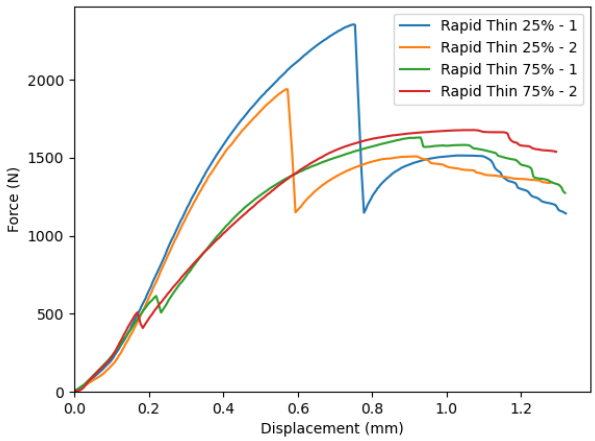
Force (N)
Displacement (mm)
Rapid Thin 25% - 1
Rapid Thin 25% - 2
Rapid Thin 75% - 1
Rapid Thin 75% - 2

f)

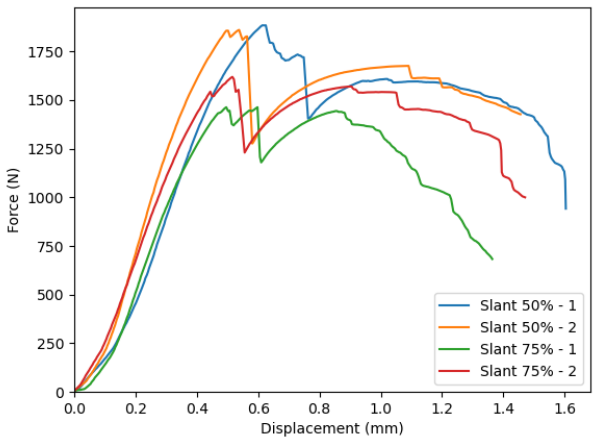
Force (N)
Displacement (mm)
Slant 50% - 1
Slant 50% - 2
Slant 75% - 1
Slant 75% - 2

g)

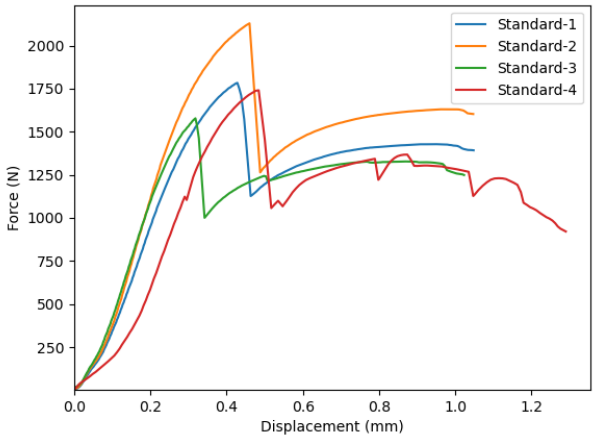
Force (N)
Displacement (mm)
Standard-1
Standard-2
Standard-3
Standard-4

h)

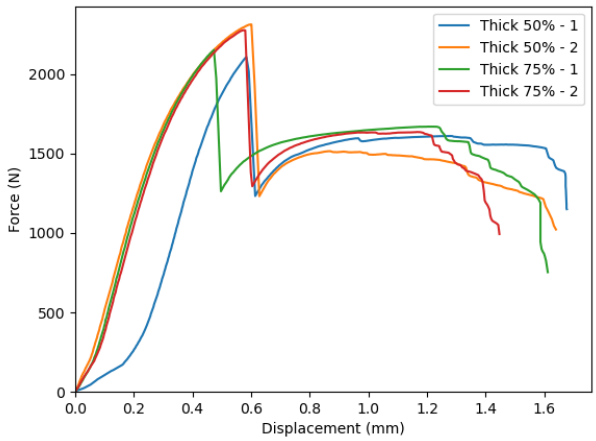

i)

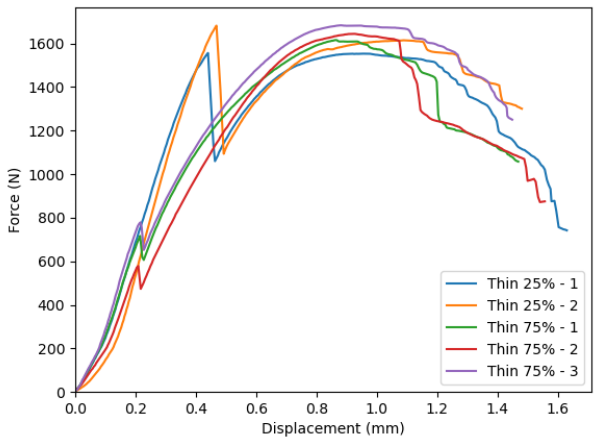

j)

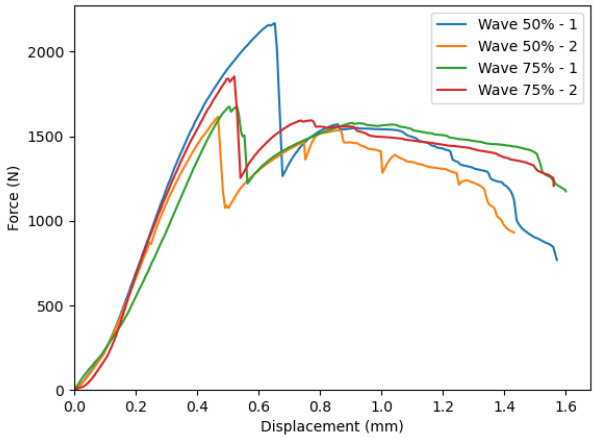

Figure 10: Force versus displacement curves for: a) centered kink lattices, b) kink+diameter change lattices, c) kink+shifted lattices, d) missing strut lattices, e) rapid thin lattices, f) slant lattices, g) standard lattices, h) extra thick lattices, i) thin lattices, j) wave lattices

It is evident that many of the defects had a large impact on the yield point. Several of the lattices behaved inconsistently with the designed experiment: wave 50% - 1, rapid thin 25% - 2, centered kink 25% 1 and 2, and the shifted kink 25% - 1. The fracture surface on each of these samples was identified to be outside of the defective region, either adjacent to the defect region or on a separate strut. The resulting force versus displacement charts resemble those of a standard or extra material lattice.

Upon inspection of the CT data, this is likely due to 25% reduction in material causing the strut to solidify in the defect region, as evidenced in Figure 11. This resulted in a reduction in the surface cracks and pores that caused failure in the other lattice samples. Similarly, the rapid thin 25% - 2, seen in Figure 12 is solid in structure compared to the surrounding strut material.

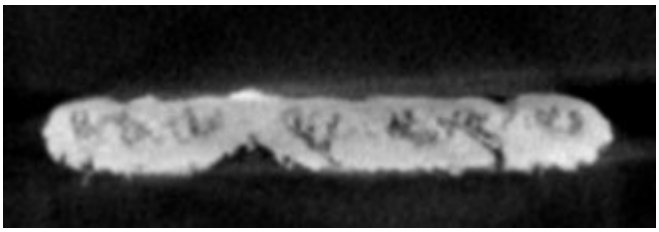

Figure 11: Slice of the CT scan for a Kink+Shifted 25% Lattice

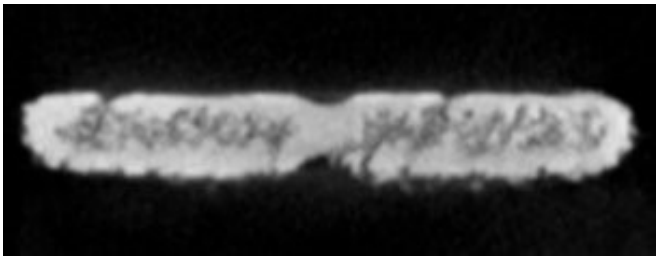

Figure 12: Slice of the CT scan for a Rapid Thin 25% Lattice

Quality factors for each defect were determined by fitting the background using a locally weighted scatterplot smoothing (LOWESS) filter [13] with a bandwidth of 0.5 and subtracting the result from the full force versus displacement curves, Figure 13. The resulting plot displays the work required to fracture the defective strut, Figure 14. Table 1 lists the resulting quality factor for each defect type, note the five anomalous results are included.

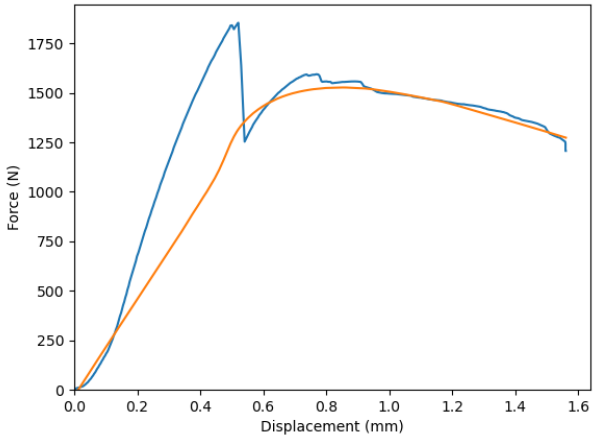

Figure 13: Locally weighted scatterplot smoothing fit to Deben CT5000RT output

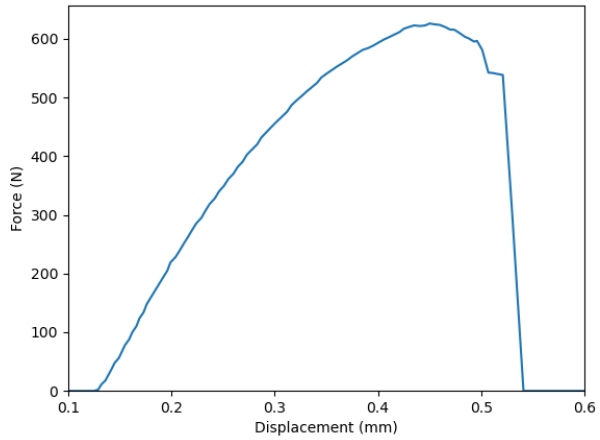

Figure 14: Measured influence of defective strut on lattice performance

Table 1: Quality Factors by Defect Type

Base	1.00
***Centered Kink 25%**	1.29
Centered Kink 75%	0.80
Kink+Diameter 25%	0.43
Kink+Diameter 50%	0.73
Kink+Shifted 25%	0.99
***Kink+Shifted 75%**	1.14
Slant 50%	1.00
Slant 75%	0.65
Thick 25%	1.34
Thick 50%	1.33
Thin 25%	0.79
Thin 75%	0.17
***Rapid Thin 25%**	1.09
Rapid Thin 75%	0.11
***Wave 50%**	0.98
Wave 75%	0.86
Missing Strut	0.00
***Anomalies Included in Results**	

These quality factors for the defective struts indicate that inspections should focus on thinned struts and rapid kinks. Excess material was found to aid in the load response, leading to the conclusion that utilizing topology optimization to reinforce regions of higher stress in parts is advantageous. Furthermore, defects of varying size and type can be attributed to a mechanical response and replaced with a straight strut of corresponding thickness to decrease FEA computational times without affecting model fidelity.

The results indicate that variability across lattice structures will continue to make qualification processes difficult until greater controls are achieved in the printing process. This study indicates that the most important factors when considering the strength of individual struts is rapid kinks and thinned struts, whether from lack of fusion, porosity, or printer variability. Future studies will focus on the minimum inspection parameters required to identify defects large enough to cause premature failure.

Variability in printing capabilities of small defects continues to be a challenge for current technology. Several of the defect types were unable to be printed, even at a 3x scaling factor. Future work will include trials to introduce microcracks by milling and filing to artificially introduce these features.

Continued efforts in this area can lead to the creation of digital twins to allow for a dramatic increase in data to be used in machine learning. Expanded datasets can help evaluate defects and predict the mechanical response, providing a useful tool for manufacturers to rapidly inspect their AM parts.

4. CONCLUSION

The results indicate that variability across lattice structures will continue to make qualification processes difficult until greater controls are achieved in the printing process. This study indicates that the most important factors when considering the strength of individual struts is rapid kinks and thinned struts, whether from lack of fusion, porosity, or printer variability. Future studies will focus on the minimum inspection parameters required to identify defects large enough to cause premature failure.

Variability in printing capabilities of small defects continues to be a challenge for current technology. Several of the defect types were unable to be printed, even at a 3x scaling factor. Future work will include trials to introduce microcracks by milling and filing to artificially introduce these features.

Continued efforts in this area can lead to the creation of digital twins to allow for a dramatic increase in data to be used in machine learning. Expanded datasets can help evaluate defects and predict the mechanical response, providing a useful tool for manufacturers to rapidly inspect their AM parts.

ACKNOWLEDGEMENTS

The authors would like to acknowledge David Moore at Sandia National Laboratory for providing guidance on previous studies using AM lattices.

This work was funded through the NNSA Office of Engineering and Technology Maturation – Advanced Manufacturing Development program. The authors would like to thank the NNSA for funding this work, as well as Katie Heroux for her leadership in managing the program.

This work was produced by Battelle Savannah River Alliance, LLC under Contract No. 89303321CEM000080 with the U.S. Department of Energy. Publisher acknowledges the U.S. Government license to provide public access under the DOE Public Access Plan (http://energy.gov/downloads/doe-public-access-plan).

REFERENCES

1) Thompson MK, Moroni G, Vaneker T, et al (2016) Design for Additive Manufacturing: Trends, opportunities, considerations, and constraints. CIRP Annals 65:737–760. doi: 10.1016/j.cirp.2016.05.004

2) Wojciechowski KW (1989) Two-dimensional isotropic system with a negative Poisson ratio. Physics Letters A 137:60–64. doi: 10.1016/0375-9601(89)90971-7

3) Mines, Jacobs (2019) Metallic microlattice structures. Springer International Publishing

4) Khosravani MR, Reinicke T (2020) On the use of X-ray computed tomography in assessment of 3D-printed components. Journal of Nondestructive Evaluation. doi: 10.1007/s10921-020-00721-1

5) Jiang P, Rifat M, Basu S (2020) Impact of surface roughness and porosity on lattice structures fabricated by additive manufacturing- A computational study. Procedia Manufacturing 48:781–789. doi: 10.1016/j.promfg.2020.05.114

6) Tammas-Williams S, Withers PJ, Todd I, Prangnell PB (2017) The influence of porosity on fatigue crack initiation in additively manufactured titanium components. Scientific Reports. doi: 10.1038/s41598-017-06504-5

7) Aloisi V, Carmignato S (2016) Influence of surface roughness on X-ray computed tomography dimensional measurements of additive manufactured parts. Case Studies in Nondestructive Testing and Evaluation 6:104–110. doi: 10.1016/j.csndt.2016.05.005

8) Hassanin H, Elshaer A, Benhadj-Djilali R, et al (2017) Surface finish improvement of additive manufactured metal parts. Micro and Precision Manufacturing 145–164. doi: 10.1007/978-3-319-68801-5_7

9) White BC, Garland A, Boyce BL (2022) Topological homogenization of metamaterial variability. Materials Today 53:16–26. doi: 10.1016/j.mattod.2022.01.021

10) Dressler AD, Jost EW, Miers JC, et al (2019) Heterogeneities dominate mechanical performance of additively manufactured metal lattice struts. Additive Manufacturing 28:692–703. doi: 10.1016/j.addma.2019.06.011

11) Kladovasilakis N, Tsongas K, Kostavelis I, et al (2021) Effective mechanical properties of additive manufactured strut-lattice structures: Experimental and finite element study. Advanced Engineering Materials 24:2100879. doi: 10.1002/adem.202100879

12) Obadimu SO, Kourousis KI (2021) Compressive behaviour of additively manufactured lattice structures: A Review. Aerospace 8:207. doi: 10.3390/aerospace8080207

13) Cleveland WS, Devlin SJ (1988) Locally weighted regression: An approach to regression analysis by local fitting. Journal of the American Statistical Association 83:596–610. doi: 10.1080/01621459.1988.10478639